Fermi-level electronic structure of a topological-insulator/cuprate-superconductor based heterostructure in the superconducting proximity effect regime

Su-Yang Xu, Chang Liu, Anthony Richardella, I. Belopolski, N. Alidoust, M. Neupane, G. Bian, Nitin Samarth, and M. Z. Hasan

Phys. Rev. B **90**, 085128 — Published 20 August 2014

DOI: 10.1103/PhysRevB.90.085128

Fermi level electronic structure of a topological insulator - cuprate superconductor based heterostructure in the proximity effect regime

Su-Yang Xu,[1] Chang Liu,[1] Anthony Richardella,[2] I. Belopolski,[1]
N. Alidoust,[1] M. Neupane,[1] G. Bian,[1] Nitin Samarth,[2] and M. Z. Hasan[1,3]

[1]*Joseph Henry Laboratory, Department of Physics, Princeton University, Princeton, New Jersey 08544, USA*
[2]*Department of Physics, The Pennsylvania State University, University Park, Pennsylvania 16802-6300, USA*
[3]*Princeton Center for Complex Materials, Princeton University, Princeton, New Jersey 08544, USA*

We probe the near Fermi level electronic structure of tunable topological insulator (Bi_2Se_3)-cuprate superconductor $Bi_2Sr_2CaCu_2O_{8+\delta}$ ($T_c \simeq 91$ K) heterostructures in their proximity induced superconductivity regime. Our careful momentum space imaging provides clear evidence for a two-phase coexistence and a striking lack of any strong *d*-wave proximity effect expected in this system. Our Fermi surface imaging data identifies key contributors in reducing the proximity-induced gap below the 5 meV or to a lower energy range ($\ll \Delta_{\rm BSCCO}$). These results correlate with our observation of momentum space separation between the Bi_2Se_3 and $Bi_2Sr_2CaCu_2O_{8+\delta}$ Fermi surface topologies and mismatch of lattice symmetries in addition to the presence of a small coherence length. These studies not only provide critical momentum space insights into the Bi_2Se_3/$Bi_2Sr_2CaCu_2O_{8+\delta}$ heterostructures, but also set an upper bound on the proximity induced gap for realizing much sought out Majorana fermion condition in this system.

I. INTRODUCTION

Topological state proximity to superconductivity (SC) has attracted much interest in condensed matter physics.[1–8] A wide range of topological quantum phenomena such as $p + ip$-wave topological superconductivity, Majorana fermions, and supersymmetry physics have been theoretically predicted, if superconductivity can be induced in the helical topological surface states of a 3D topological insulator (TI). These phenomena are of great interest both in fundamental physics since they serve as a novel bridge between high energy and condensed matter physics and in applicative purposes because realization of Majorana fermions in a condensed matter setting can be used to build the basic qubit for a topological quantum computer.

In contrast to idealized theoretical models[1,4] where only Dirac surface states cross the Fermi level, real TI/SC samples exhibit a complex phenomenology due to the coexistence of topological surface states and bulk conduction bands at the chemical potential. Thus although progress has been reported by using conventional transport and STM experiments[9–26], those studies do not have the momentum resolution necessary to distinguish the contribution to the STM or transport signals of the topological surface states from that of the bulk or impurity bands. In fact, it has been recently shown[27–30] that the undesirable superconductivity in the bulk and impurity bands can lead to ambiguous interpretation of the transport and STM data regarding Majorana fermions. Therefore, in order to realize any of the fascinating theoretical proposals, it is of importance to systematically study the near Fermi level electronic structure in a *momentum(band)-resolved* manner of the heterostructure sample between a topological insulator and a superconductor, in its proximity induced superconducting regime. This is because that without an understanding of the near Fermi level electronic structure in a *momentum(band)-resolved* manner of a certain TI/SC heterostructure sample, it is not possible to interpret any STM or transport data on that particular sample without any ambiguity due to the bulk or impurity band[27–30], and it is further not possible to construct or optimize a TI/SC sample where the superconductivity from the topological surface states dominates and the exciting new physics could be finally realized.

Among all known superconductors, the high-temperature cuprate superconductor $Bi_2Sr_2CaCu_2O_{8+\delta}$ (BSCCO) possesses one of the highest superconducting transition temperature ($T_c \sim 91$ K for the optimally doped composition) and one of the largest superconducting gap values ($\Delta \gtrsim 30$ meV). These properties make the TI/BSCCO heterostructure a quite promising candidate for a very strong superconducting proximity effect in the topological surface states. A strong proximity effect means that the proximity-induced superconductivity in the TI surface states exhibits a large superconducting gap at a relatively high temperature. These are critical conditions for realizing a stable Majorana fermion[1] or the emergent supersymmetry phenomenon[8] for experimental detection. Therefore, in order to understand the superconducting proximity effect in the helical surface states in the Bi_2Se_3/$Bi_2Sr_2CaCu_2O_{8+\delta}$ heterostructure, it is important to carefully study the electronic structure of the Bi_2Se_3 film in a *momentum(band)-resolved* manner. In this paper, we report fabrication of delicate heterostructure samples between topological insulator (TI) Bi_2Se_3 thin film and high temperature superconductor optimally doped $Bi_2Sr_2CaCu_2O_{8+\delta}$ ($T_c \simeq 91$ K). Using angle-resolved photoemission spectroscopy, we momentum-resolve the electronic structure and

the possible superconducting gap on the top surface of Bi_2Se_3 thin films. Our systematic data provides clear evidence for a two-(crystalline orientation) phase coexistence, and a lack of *d*-wave-like proximity effect in contrast to a previous report.[31] Our Fermi surface imaging data identifies major contributors in reducing the proximity-induced gap to below the 5 meV range. These results correlate with our observation of momentum space separation between the Bi_2Se_3 and $Bi_2Sr_2CaCu_2O_{8+\delta}$ Fermi surfaces and mismatch of crystalline symmetries in the presence of a small superconducting coherence length. These studies not only provide critical momentum space insights into the $Bi_2Se_3/Bi_2Sr_2CaCu_2O_{8+\delta}$ heterostructures, but also set an upper bound on the proximity induced gap for realizing much sought out Majorana fermion condition in this system.

II. METHODS

Single crystalline samples of optimally doped $Bi_2Sr_2CaCu_2O_{8+\delta}$ with $T_c \simeq 91$ K were grown using the standard method.[32] The BSCCO crystals were cleaved *in situ* under ultra-high vacuum, and high quality topological insulator Bi_2Se_3 thin films were then grown by the molecular beam epitaxy (MBE) on top of freshly cleaved surface of BSCCO. The MBE growth utilized thermal evaporation from high purity elemental Knudsen cells under selenium rich conditions. During the growth, the Se shutter was opened for 30 seconds before opening the Bi shutter. No clear change can be seen in the RHEED pattern from the BSCCO when it was exposed to Se. This indicates that there is not a strong reaction with Se. In order to protect the surface at the ambient pressure, a thick $\sim$ 50 nm selenium (Se) capping layer was deposited on the Bi_2Se_3 thin film immediately after the growth by continuing the selenium source evaporation while the film cooled to room temperature. The Se capping layer can be removed by heating the sample *in situ* in the ARPES chamber at $\sim$ 200 °C for about an hour, as reported in Ref.[31,33]. High-resolution ARPES measurements were performed at the beamlines 4.0.3 and 10.0.1 at the Advanced Light Source (ALS) in the Lawrence Berkeley National Laboratory (LBNL) in Berkeley, CA. The base temperature and base pressure of the ARPES beamlines at the ALS were about 10 K and $< 5 \times 10^{-11}$ torr, and the total energy and momentum resolution of these beamlines were about 15 meV and 0.01 $Å^{-1}$. The kinetic energy of the Fermi level was determined by fitting the ARPES spectrum of gold to the Fermi-Dirac distribution function at 10 K convolved with a gaussian function (Fig. 1b). The existence of SC gap is determined by comparing the leading edge energy shift between the energy distribution curve (EDC) in the data and the EDC in the gold spectrum. Therefore, the stability of the kinetic energy of the Fermi level over time defines the ability and stability of measuring leading-edge energies (therefore the superconducting gap).[34] We have checked the stability of the kinetic energy of the Fermi level by measuring the gold spectra over time, and have found the fluctuation of the Fermi level to be less than 2 meV in the normal running mode of the ARPES machines (Fig. 1c and Fig. 2), at which our data on Bi_2Se_3/BSCCO films were collected. From that, we conservatively set the upper bound of SC gap at a level less than 5 meV.

III. RESULTS AND DISCUSSION

Fig. 1a shows the experimental configuration. Topological insulator Bi_2Se_3 thin films at various thicknesses were grown on top of freshly cleaved surface of BSCCO crystals. ARPES experiments were then performed to measure the electronic structure on the top surface of the Bi_2Se_3 films. Fig. 1d shows the energy-momentum dispersion of a 6 quintuple layer (QL) thick Bi_2Se_3 film sample on the BSCCO. A single-Dirac cone surface state centered at the $\bar{\Gamma}$ point is observed. No Dirac point gap is seen, which indicates that the 6 QL film is above the limit at which the two surfaces couple to each other, consistent with the previous report.[35,36] Fermi surface mapping over a wide momentum-space window is shown in Fig. 1e. Interestingly, the two nearby second BZ Fermi surfaces are found to be only 30° rotated with respect to each other, which demonstrates that there exist two sets of BZs that are 30° rotated. In real space, this observation means that the film contains two sets of crystalline (phases) domains that are 30° rotated. We note that the ARPES Fermi surface in Fig. 1e is reproducible and always contains these two sets of domains, as the beamspot is moved at different positions on a film surface. Thus the size of the domains must be intrinsically smaller than that of the beamspot (50 μm $\times$ 100 μm). The coexistence of two sets of domains is a reasonable consequence considering the different lattice symmetries (square vs hexagonal) in the BSCCO substrate and the Bi_2Se_3 film.

The existence of SC gap is determined by comparing the leading edge energy shift between the energy distribution curve (EDC) in the data and the EDC in the gold spectrum. Therefore, the stability of the kinetic energy of the Fermi level over time defines the capability and stability of measuring leading-edge energies (therefore the superconducting gap).[38] We have checked the stability of the kinetic energy of the Fermi level by measuring the gold spectra over time, and have found the fluctuation of the Fermi level to be less than 2 meV in the normal running mode of the ARPES machines (Fig. 2). From that, we conservatively set our confidence level at 5 meV. We also note that, beside the method of comparing the leading edge shift, another commonly used way to determine the SC gap is by fitting the ARPES data using Dynes[39] or BSC[40] spectral function. However, it is well-known

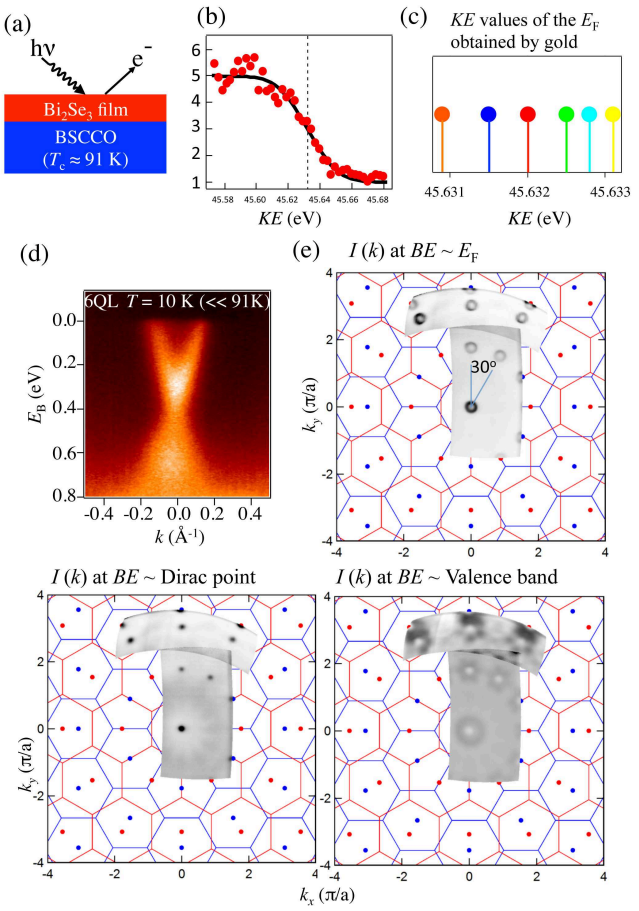

FIG. 1: **Characterization of Bi_2Se_3/BSCCO film heterostructure systems.** (a) Schematic illustration of our experimental configuration. (b) A gold spectrum (red circles) and its Fermi-Dirac fit (black line) measured at $T = 10$ K at photon energy of 50 eV. (c) Kinetic energy values of the Fermi level determined by gold spectrum measurements at $T = 10$ K at photon energy of 50 eV, at various time points during our data collection. (d) ARPES dispersion map of a 6 QL Bi_2Se_3 film sample on BSCCO. (e) ARPES Fermi surface map of a 6 QL Bi_2Se_3 film sample over a wide momentum space range superimposed on top of a schematic drawing of two sets of Bi_2Se_3 surface Brillouin zones (BZs), which are 30° rotated with respect to each other.

that the SC gaps in high temperature superconductors such as BSCCO are not well described by those functions that utilize conventional s-wave BCS cooper pairing mechanism. Furthermore, we are dealing with the proximity superconducting effect induced by the d-wave superconducting substrate, and therefore using Dynes or BCS function is even less reliable. On the other hand, we believe the method of comparing the leading edge shift that we applied is more appropriate and sufficient considering the issue we are dealing with and the confidence level we set. Taking 2 meV (upper limit of the Fermi level fluctuation) as the standard error σ, to reach a confidence level of 95%, the confidence interval is determined by $1.96\frac{\sigma}{\sqrt{(n)}}$. Considering that we show data on two samples, we can take $n = 2$. But here we choose the even safer approach as $n = 1$. Therefore the upper bound of SC gap is $1.96 \times 2 \simeq 4$ meV. From that, we conservatively set the upper bound of SC gap at a level less than 5 meV.

We now study the low energy electronic structure at various temperatures across the T_c of BSCCO, in order to search for possible existence of superconducting gap in the topological surface states. The blue arrow in Fig. 3a denotes the momentum where the topological surface states cross the Fermi level. The ARPES EDC data at the momentum indicated by the blue arrow at various temperatures are shown in Fig. 3b. No leading-edge shift (energy gap at the Fermi level) nor superconducting coherence peak is observed as temperature is raised from 10 K (below the T_c of BSCCO) to 100 K (above the T_c of BSCCO). To exclude any systematic error or artifacts, the sample is re-cooled down from 100 K to 10 K. However, again no superconducting gap is observed (Fig. 3c).

Since the 6 QL film is above the surface-to-surface coupling thickness threshold, we also study a 3 QL Bi_2Se_3 sample as shown in Fig. 4. Fig. 4a shows the surface state dispersion. A gap at the Dirac point is clearly observed in the 3 QL sample, which shows that at 3 QL the top and bottom surface states are coupled to each other. Temperature dependent ARPES measurements are done at the momentum where surface states cross the Fermi level. As shown in Fig. 4b, no superconducting gap is found, which demonstrates that even at 3 QL no observable superconducting gap larger than 5 meV exists in the surface states localized near the top surface. We note that our experiments are performed with similar or better conditions than that reported in Ref.[31].

We note that a recent photoemission experiment has drawn particular attention because it reported the observation of a large gap ($\simeq$ 15 meV) in the electron-quasiparticle density of states (interpreted as the superconducting gap) in the surface states of TI Bi_2Se_3 films (even as thick as 7 quintuple layer $\simeq$ 7 nm) grown on top of a d-wave high temperature superconductor $Bi_2Sr_2CaCu_2O_{8+\delta}$ (BSCCO).[31] However, the gap in Ref.[31] was found to show unusual behaviors, such as the absence of an observable superconducting coherence peak (a critical, decisive, and indispensable signature for a superconducting gap) and a strong k_z dependence of the magnitude of the gap (note that BSCCO is almost ideally (quasi-)2D and the topological surface state is also a 2D state). This behavior reported in Ref.[31] is inconsistent with the physical picture of the superconducting proximity effect. Here, our careful and systematic ARPES measurements clearly exclude the existence of superconducting gap in the helical surface states of Bi_2Se_3 larger than 5 meV, in contrast to the previous result in Ref.[31]. Further ultra-high resolution and ultra-low temperature ARPES measurements are required to resolve the existence of a small ($\leq$ 5 meV) or even sub-meV supercon-

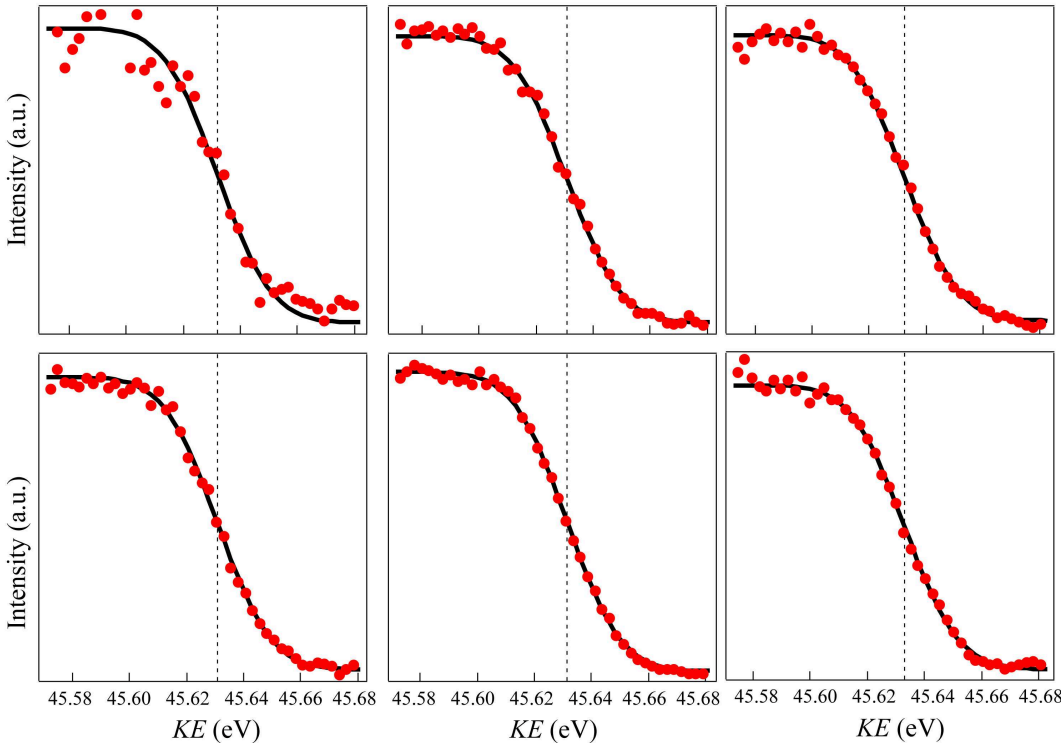

FIG. 2: **Gold spectra showing the stability of the Fermi level.** Gold spectra at $T = 10$ K at photon energy of 50 eV taken at various time points during our data collection. These gold measurements show that the fluctuation of the Fermi level was found to be less than 2 meV in the normal running mode of the ARPES machines.

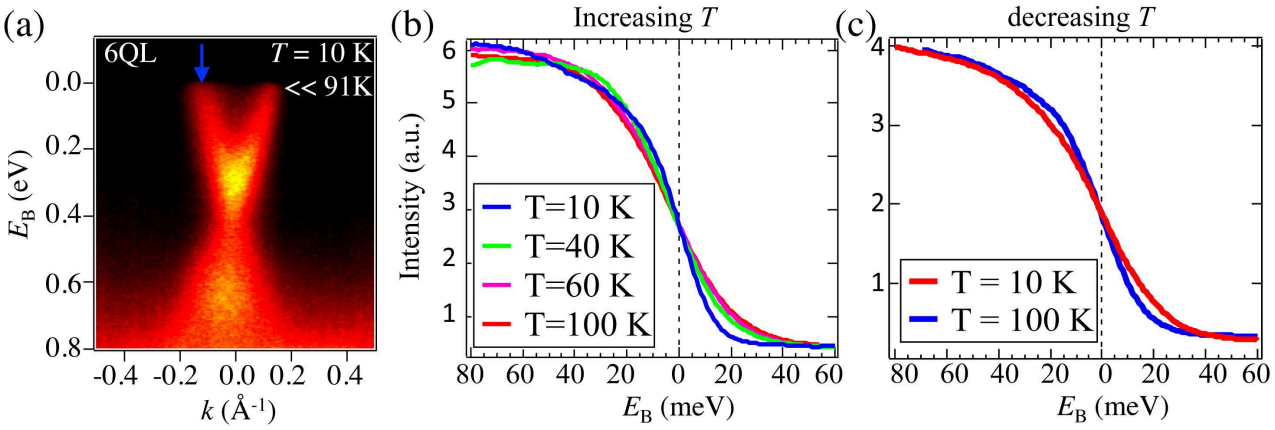

FIG. 3: **Temperature dependent ARPES data on a 6 QL Bi_2Se_3/BSCCO sample.** (a) ARPES dispersion map of a 6 QL Bi_2Se_3/BSCCO using photon energy of 50 eV. The blue arrow notes the momentum chosen for detailed temperature dependent studies. (b and c) ARPES energy distribution curve (EDC) data at different temperatures. For the dataset with increasing (decreasing) temperature, the measurements were taken using incident photon energy of 50 eV (55 eV).

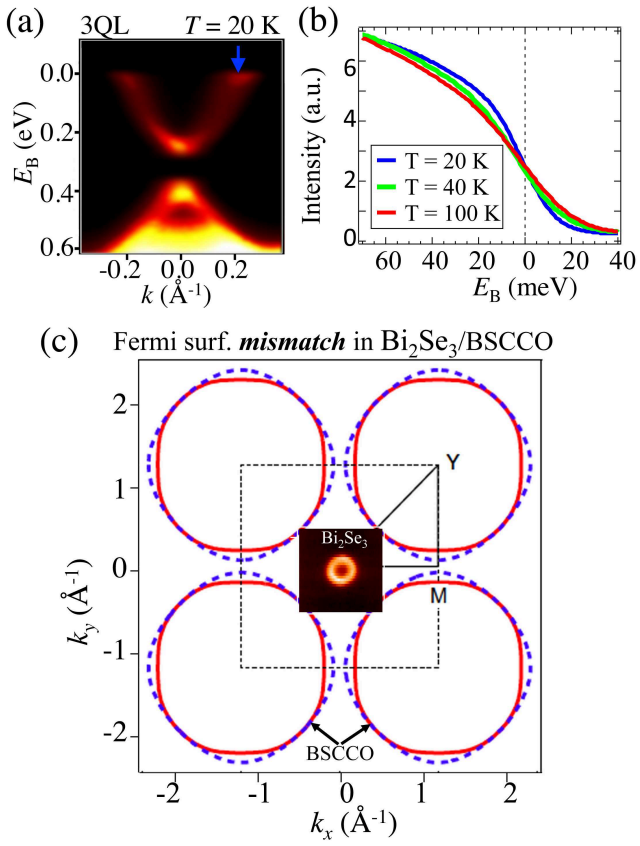

FIG. 4: **Temperature dependent ARPES data on a 3 QL Bi_2Se_3/BSCCO sample.** (a) Dispersion map of a 3 QL Bi_2Se_3/BSCCO sample usingphoton energy of 60 eV. The blue arrow notes the momentum chosen for detailed temperature dependent studies. (b) ARPES energy distribution curve (EDC) data ($h\nu = 70$ eV) at different temperatures. (c) ARPES Fermi surface mapping of a 6 QL Bi_2Se_3 film sample superimposed on top of a schematic BSCCO Fermi surface. The two Fermi surfaces are shown using the same momentum-axes. The BSCCO Fermi surface schematic is adapted from Ref.[41].

ducting gap exists in the surface states and its magnitude. We identify the following contributors based on our data in reducing the proximity-induced superconducting gap to below the 5 meV range. First, our observation of the coexistence of two-crystalline-domains (phases) rotated by 30 degrees demonstrate the fact that the strong mismatch of lattice symmetries between Bi_2Se_3 and BSCCO limits the quality of the interface, which is unfavorable for the large amplitude Cooper pair tunneling at the heterostructure interface, severely limiting the magnitude of proximity effect. Second, as seen in Fig. 4c, BSCCO has four pieces of Fermi surface at the Brillouin zone (BZ) corner whereas Bi_2Se_3 features one small surface Fermi surface at the surface BZ center. Therefore, the lack of momentum space overlap between their Fermi surfaces also make it difficult for the Cooper pairs tunneling across the interface. Third, the nodal d-wave superconducting order parameter in BSCCO is different from the theoretically expected $p + ip$ wave (isotropic SC gap, nodeless) superconductivity in TIs.[1] The different pairing symmetries and (nodal/nodeless) nature of the SC gap make the TI/BSCCO interface further unsuitable for a strong superconducting proximity effect. Finally, BSCCO and other cuprate superconductors are known to have a short superconducting coherence length, especially along the out-of-plane direction (only less than 1 nm).[37] Thus even if the above conditions (lattice symmetries, k_F, superconducting order parameters and pairing symmetries) between these two systems could be perfectly matched, the proximity induced superconductivity is not expected to propagate over a distance (film thickness larger than 1 or 2 QL) along the c-axis of BSCCO. In addition to these factors, the d-wave superconductivity in BSCCO can further destabilize the Majorana fermions at the interface, since Majorana modes can leak to the BSCCO substrate through the nodes (gapless) of the superconducting gap, causing dephasing or decoherence of the zero-bias modes. Therefore, Our finding establishes a stringent criterion on proximity-induced SC gap by high temperature superconductor, indicating that it is difficult, if possible, to realize Majorana fermion in the d-wave proximity settings.

Apart from absence of observable superconducting gap in the surface states, the observed two micro-crystalline-domains that are 30° rotated in Bi_2Se_3 worths further investigation using probes with space resolution such as STM. Furthermore, the coexistence of two domains also means that in a space-average probe such as ARPES, the $\bar{\Gamma} - \bar{M}$ and $\bar{\Gamma} - \bar{K}$ directions are now equivalent because these two directions from the two domains are mapped onto each other (Fig. 1e). Therefore, any possible anisotropy ($p_x + ip_y$) in the superconducting gap is further smeared out in ARPES measurements. Finally, it would be particularly exciting to study the proximity effect of the pseudo-gap states in the under-doped BSCCO system by searching for pseudo-gap in the Bi_2Se_3 surface states in energy scale of small sub 5 meV.

IV. CONCLUSION

In conclusion, we have systematically studied the near Fermi level electronic structure of thin film topological insulator (Bi_2Se_3)-cuprate superconductor $Bi_2Sr_2CaCu_2O_{8+\delta}$ ($T_c \simeq 91$ K) heterostructures. These TI/SC interface-samples are believed to be one of the most promising platforms for realizing novel fundamental physics such as supersymmetry phenomenon and Majorana fermions, and therefore it is in this context that our systematic studies on their near Fermi level electronic structure in the proximity superconductivity regime is of critical importance. Our careful momentum space imaging have provided clear evidence for a two-phase coexistence and a striking lack of any strong d-wave proximity effect by setting up an upper bound of the proximity su-

perconducting gap of 5 meV ($\ll \Delta_{\rm BSCCO}$). These studies have provided critical insights for realizing much sought out Majorana fermion condition in this system.

ACKNOWLEDGEMENT: The work at Princeton was supported by Office of Basic Energy Science, US Department of Energy (grant DE-FG-02-05ER46200/Hasan). The MBE synthesis at Penn State University was supported by the ARO MURI program. We gratefully thank G. Gu and H. Eisaki for sharing the BSCCO samples.

Note added: Finally, we note that while finalizing our manuscript, another group also reported the lack of strong superconducting proximity effect in the TI/BSCCO heterostructure samples[42] but the coexistence of two-phase (as observed in our manuscript) was not reported.

[1] L. Fu and C. L. Kane, Phys. Rev. Lett. **100**, 096407 (2008).
[2] M. Z. Hasan and C. L. Kane, Rev. Mod. Phys. **82**, 3045-3067 (2010).
[3] X. -L. Qi and S. -C. Zhang, Rev. Mod. Phys. **83**, 1057-1110 (2011).
[4] X.-L. Qi, T. L. Hughes, S. Raghu, S.-C. Zhang, Phys. Rev. Lett. **102**, 187001 (2009).
[5] J. Linder, Y. Tanaka, T. Yokoyama, A. Sudbø, N. Nagaosa, Phys. Rev. Lett. **104**, 067001 (2010).
[6] A. C. Potter and P. A. Lee, Phys. Rev. B **83**, 184520 (2011).
[7] J. D. Sau, Roman M. Lutchyn, S. Tewari, S. Das Sarma, Phys. Rev. Lett. **104**, 040502 (2010).
[8] T. Grover, D. N. Sheng, A. Vishwanath, Science **344**, 280 (2014).
[9] Y. S. Hor, A. J. Williams, J. G. Checkelsky, P. Roushan, J. Seo, Q. Xu, H. W. Zandbergen, A. Yazdani, N. P. Ong, R. J. Cava, Phys. Rev. Lett. **104**, 057001 (2010).
[10] S. Sasaki, M. Kriener, K. Segawa, K. Yada, Y. Tanaka, M. Sato, Y. Ando, Phys. Rev. Lett. **107**, 217001 (2011).
[11] D. Zhang, J. Wang, A. M. DaSilva, J. Sue Lee, H. R. Gutierrez, M. H. W. Chan, J. Jain, N. Samarth, Phys. Rev. B **84**, 165120 (2011).
[12] G. Koren, T. Kirzhner, E. Lahoud, K. B. Chashka, A. Kanigel, Phys. Rev. B **84**, 224521 (2011).
[13] B. Sacépé, J. B. Oostinga, J. Li, A. Ubaldini, N. J. G. Couto, E. Giannini, A. F. Morpurgo, Nature Commun. **2**, 575 (2011).
[14] F. Qu, F. Yang, J. Shen, Y. Ding, J. Chen, Z. Ji, G. Liu, J. Fan, X. Jing, C. Yang, Li Lu, Scientific Reports **2**, 339 (2012).
[15] S. Cho, B. Dellabetta, A. Yang, J. Schneeloch, Z. Xu, T. Valla, G. Gu, M. J. Gilbert, N. Mason, Nature Commun. **4**, 1689 (2013).
[16] F. Yang, F. Qu, J. Shen, Y. Ding, J. Chen, Z. Ji, G. Liu, J. Fan, C. Yang, L. Fu, L. Lu, Phys. Rev. B **86**, 134504 (2012).
[17] J. R. Williams, A. J. Bestwick, P. Gallagher, S. S. Hong, Y. Cui, A. S. Bleich, J. G. Analytis, I. R. Fisher, D. Goldhaber-Gordon, Phys. Rev. Lett. **109**, 056803 (2012).
[18] M.-X. Wang, C. Liu, J.-P. Xu, F. Yang, L. Miao, M.-Y. Yao, C. L. Gao, C. Shen, X. Ma, X. Chen, .Z-A. Xu, Y. Liu, S.-C. Zhang, D. Qian, J.-F. Jia, Q.-K. Xue, Science **336**, 52-55 (2012).
[19] M. Veldhorst, M. Snelder, M. Hoek, T. Gang, V. K. Guduru, X. L. Wang, U. Zeitler, W. G. van der Wiel, A. A. Golubov, H. Hilgenkamp, A. Brinkman, Nature Mater. **11**, 417 (2012).
[20] P. Zareapour, A. Hayat, S. Yang, F. Zhao, M. Kreshchuk, A. Jain, D. C. Kwok, N. Lee, S.-W. Cheong, Z. Xu, A. Yang, G. D. Gu, S. Jia, R. J. Cava, K. S. Burch, Nature Commun. **3**, 1056 (2012).
[21] L. Maier, J. B. Oostinga, D. Knott, C. Büne, P. Virtanen, G. Tkachov, E. M. Hankiewicz, C. Gould, H. Buhmann, L. W. Molenkamp, Phys. Rev. Lett. **109**, 186806 (2012).
[22] G. Koren and T. Kirzhner, Phys. Rev. B **86**, 144508 (2012).
[23] G. Koren, T. Kirzhner1, Y. Kalcheim, O. Millo, Euro. Phys. Lett. **103**, 67010 (2013).
[24] J.-P. Xu, C. Liu, M.-X. Wang, J. Ge, Z.-L. Liu, X. Yang, Y. Chen, Y. Liu, Z.-A. Xu, C.-L. Gao, D. Qian, F.-C. Zhang, J.-F. Jia, Phys. Rev. Lett. **112**, 217001 (2014).
[25] V. Mourik, K. Zuo, S. M. Frolov, S. R. Plissard, E. P. A. M. Bakkers, L. P. Kouwenhoven, Science **336**, 1003-1007 (2012).
[26] A. Das, Y. Ronen, Y. Most, Y. Oreg, M. Heiblum, H. Shtrikman, Nature Phys. **8**, 887-895 (2012).
[27] J. Liu, A. C. Potter, K. T. Law, P. A. Lee, Phys. Rev. Lett. **109**, 267002 (2012).
[28] D. Roy, N. Bondyopadhaya, S. Tewari, Phys. Rev. B **88**, 020502(R) (2013).
[29] H. O. H. Churchill, V. Fatemi, K. Grove-Rasmussen, M. T. Deng, P. Caroff, H. Q. Xu, C. M. Marcus, Phys. Rev. B **87**, 241401(R) (2013).
[30] E. J. H. Lee, X. Jiang, M. Houzet, R. Aguado, C. M. Lieber, S. D. Franceschi, Nature nanotech. **9**, 79 (2014).
[31] E. Wang, H. Ding, A. V. Fedorov, W. Yao, Z. Li, Y.-F. Lv, K. Zhao, L.-G. Zhang, Z. Xu, J. Schneeloch, R. Zhong, S.-H. Ji, L. Wang, K. He, X. Ma, G. Gu, H. Yao, Q.-K. Xue, X. Chen, S. Zhou, Nature Phys. **9**, 621 (2013).
[32] G. D. Gu, K. Takamuku, N. Koshizuka, S. Tanaka, J. Cryst. Growth **137**, 472 (1994).
[33] S.-Y. Xu, M. Neupane, C. Liu, D. Zhang, A. Richardella, L. A. Wray, N. Alidoust, M. Leandersson, T. Balasubramanian, J. Sánchez-Barriga, O. Rader, G. Landolt, B. Slomski, J. H. Dil, J. Osterwalder, T.-R. Chang, H.-T. Jeng, H. Lin, A. Bansil, N. Samarth, M. Z. Hasan, Nature Phys. **8**, 616 (2012).
[34] We note that it is the stability of the Fermi level over time, not the energy resolution of the ARPES machine, that defines the ability and stability of measuring the superconducting gap. Finite energy resolution can Gaussian-broaden the data feature, but it is not expected to shift the energy position of the leading edge. Thus the 15 meV energy resolution is not directly related to the ability of measuring superconducting gap. The fluctuation of Fermi level over time (tracked by measuring gold spectra over time) is found to be maximally 2 meV. From that, we (conservatively) can set 5 meV upper bound for the SC gap.
[35] Y. Zhang, K. He, C.-Z. Chang, C.-L. Song, L.-L. Wang,

X. Chen, J.-F. Jia, Z. Fang, X. Dai, W.-Y. Shan, S.-Q. Shen, Q. Niu, X.-L. Qi, S.-C. Zhang, X.-C. Ma, Q.-K. Xue, Nature Phys. **6**, 584-588 (2010).

[36] M. Neupane, A. Richardella, J. Sánchez-Barriga, S.-Y. Xu, N. Alidoust, I. Belopolski, C. Liu, G. Bian, D. Zhang, D. Marchenko, A. Varykhalov, O. Rader, M. Leandersson, T. Balasubramanian, T.-R. Chang, H.-T. Jeng, S. Basak, H. Lin, A. Bansil, N. Samarth, M. Z. Hasan, Nature Commun. **5**, 4841 (2014).

[37] W. Lang, G. Heine, W. Kula, R. Sobolewski, Phys. Rev. B **51**, 9180 (1995).

[38] T. Kiss, T. Yokoya, A. Chainani, S. Shin, T. Hanaguri, M. Nohara, H. Takagi, Nature Phys. **3**, 720 (2007).

[39] R. C. Dynes, V. Narayanamurti, J. P. Garno, Phys. Rev. Lett. **41**, 1509 (1978).

[40] H. Matsui, T. Sato, T. Takahashi, S.-C. Wang, H.-B. Yang, H. Ding, T. Fujii, T. Watanabe, A. Matsuda, Phys. Rev. Lett. **90**, 217002 (2003).

[41] A. A. Kordyuk, S. V. Borisenko, M. Knupfer, J. Fink, Phys. Rev. B **67**, 064504 (2003).

[42] T. Yilmaz, I. Pletikosic, A. P. Weber, J. T. Sadowski, G. D. Gu, A. N. Caruso, B. Sinkovic, T. Valla, arXiv:1403.4184 (2014).